The off-axis pressure crash associated with the nonlinear evolution of the m/n=2/1 double tearing mode

W. Zhang[1], X. Lin[1], Z. W. Ma[1,*], X. Q. Lu[2] , and H. W. Zhang[1]

[1]Institute for Fusion Theory and Simulation, Department of Physics, Zhejiang University, Hangzhou 310027, China

[2]College of Nuclear Equipment and Nuclear Engineering, Yantai University, Yantai 264005, China

Abstract: The nonlinear evolution of the m/n=2/1 double tearing mode (DTM) is investigated by the toroidal resistive magnetohydrodynamic code CLT. It is found that the m/n=2/1 DTM can lead to the core pressure crash and the off-axis pressure crash. Unlike the core pressure crash, the plasma pressure at the magnetic axis keeps almost unchanged during the off-axis pressure crash. The pressure crash only occurs in the annular region during the off-axis crash, and the on-axis plasma pressure slowly reduces after the crash, which is well consistent with TFTR observations. A series of simulations are carried out to investigate the influence of the radial position of the inner resonant surface r_1 , the magnetic shear at the inner resonance surface, and the spatial separation between the two resonant surfaces on the nonlinear behavior of the DTM. We find that r_1 is the dominant factor for the two different kinds of the nonlinear DTM behaviors. For a smaller r_1 , the magnetic flux inside the inner resonant surface is less, and the DTM leads to a core pressure crash and vice versa. It is also found that the magnetic shear at the inner resonant surface and the distance between the two resonant surfaces can also influence the critical r_1 for the two kinds of nonlinear DTM behaviors. A simple theoretical formula of the transition criterion between the two pressure crashes is proposed, which agrees well with the simulation results.

[a)] Corresponding Author: zwma@zju.edu.cn

I. Introduction

It is widely believed that the reversed q profile can help to stabilize the drift instabilities[1], the ballooning instability[2], and the electron temperature gradient turbulence[3] in Tokamaks. The reversed q profile is also crucial for the formation of the internal transport barrier (ITB), which can significantly improve the energy confinement of Tokamaks. [4-6] This widely adopted profile in advanced Tokamaks[3, 7-9] has also been considered as one of the advanced operational scenarios in future fusion reactors.[10, 11] However, with a reversed q profile, there exists a destructive MHD instability-the double tearing mode (DTM) instability.[12-37] DTM develops much faster than a single tearing mode and can lead to a significant crash of the central plasma pressure.[38-41]

As shown in TFTR[38], there are two different kinds of pressure crashes associated with the nonlinear evolution of the m/n=2/1 DTM. One is called the off-axis pressure crash, during which the pressure crash only occurs in the annular region, and the plasma pressure at the magnetic axis remains almost unchanged. Another is called the core pressure crash, in which the pressure crash occurs in the whole core region, and the plasma pressure at the magnetic axis is significantly reduced. Since they are both dangerous for Tokamaks, many simulation and theoretical studies have been done ever since they were observed.[12, 15, 16, 34, 38, 42, 43] However, it is still unclear which parameter is the dominant one to lead to the two different kinds of pressure crashes. In the present paper, a systematical investigation of the m/n=2/1 DTM and the transition condition between the core and off-axis pressure crash are presented.

II. Model description

The compressible resistive-magnetohydrodynamic (MHD) equations used in CLT are given as follows:

$$\frac{\partial \rho}{\partial t} = -\nabla \cdot (\rho \mathbf{v}) + \nabla \cdot [D \nabla (\rho)], \tag{1}$$

$$\frac{\partial p}{\partial t} = -\mathbf{v}\cdot\nabla p - \Gamma p\nabla\cdot\mathbf{v} + \nabla\cdot[\kappa_{\perp}\nabla(p)] + \nabla\cdot[\kappa_{\parallel}\nabla_{\parallel}p], \tag{2}$$

$$\frac{\partial \mathbf{v}}{\partial t} = -\mathbf{v}\cdot\nabla\mathbf{v} + (\mathbf{J}\times\mathbf{B} - \nabla p)/\rho + \nabla\cdot[\nu\nabla(\mathbf{v})], \tag{3}$$

$$\frac{\partial \mathbf{B}}{\partial t} = -\nabla\times\mathbf{E}, \tag{4}$$

$$\mathbf{E} = -\mathbf{v}\times\mathbf{B} + \eta\mathbf{J}, \tag{5}$$

$$\mathbf{J} = \frac{1}{\mu_0}\nabla\times\mathbf{B}, \tag{6}$$

Where ρ, p, **v**, **B**, **E**, and **J** are the plasma density, the plasma pressure, the fluid velocity, the magnetic field, the electric field, and the current density, respectively. $\Gamma(=5/3)$ is the ratio of specific heat of the plasma. Different from the traditional single-fluid equations, the electric field is used as an intermediate variable to keep $\nabla\bullet\mathbf{B}=0$. The variables are normalized as follows: $\rho/\rho_{00}\to\rho$, $\mathbf{x}/a\to\mathbf{x}$, $\mathbf{B}/B_{00}\to\mathbf{B}$, $\mathbf{v}/v_A\to\mathbf{v}$, $t/t_A\to t$, $\mathbf{E}/(v_A B_{00})\to\mathbf{E}$, $\mathbf{J}/(B_{00}/\mu_0 a)\to\mathbf{J}$, and, $p/(B_{00}^2/\mu_0)\to p$,where a is the minor radius, $v_A = B_{00}/\sqrt{\mu_0\rho_{00}}$ is the Alfvén speed, and $t_A = a/v_A$ is the Alfvén time. B_{00} and ρ_{00} are the initial magnetic field and plasma density at the magnetic axis, respectively. η, D, $\kappa_{\perp}$, $\kappa_{\parallel}$, and υ are the resistivity, the plasma diffusion coefficient, the parallel, and perpendicular thermal conductivity, and the viscosity, respectively. They are normalized as follows: $\eta/(\mu_0 a^2/t_A)\to\eta$, $D/(a^2/t_A)\to D$, $\kappa_{\parallel}/(a^2/t_A)\to\kappa_{\parallel}$, $\kappa_{\perp}/(a^2/t_A)\to\kappa_{\perp}$, and $\nu/(a^2/t_A)\to\nu$, respectively.

III. Simulation results

A. Off-axis pressure crash

Since the purpose of the present paper is to investigate the off-axis pressure crash

observed in TFTR[38], the parameters of TFTR are used, i. e., the major radius ($R_0 = 2.60m$), the minor radius ($a = 0.94m$) for a circular cross-section geometry. The initial safety factor and plasma pressure profiles used in the subsection is shown in Figure 1. The function of the safety factor profile is given as

$$q(r) = q_0[1+(\psi / r_0^2)^{\lambda}]^{1/\lambda}[1+A\exp(-\psi/\delta^2)]/(1+A), \tag{7}$$

where ψ is the normalized poloidal magnetic flux, $q_0 = 4.5$ is the safety factor at the magnetic axis, r_0=0.612 , λ=6.48 , $A = 1.64$, and $\delta = 0.23$. With these parameters, the minimum safety factor is $q_{\min} = 1.75$. The function of the pressure profile is

$$p = p_0(1-\psi), \tag{8}$$

where the plasma pressure at the magnetic axis is fixed to be $p_0 = 0.722\%$.

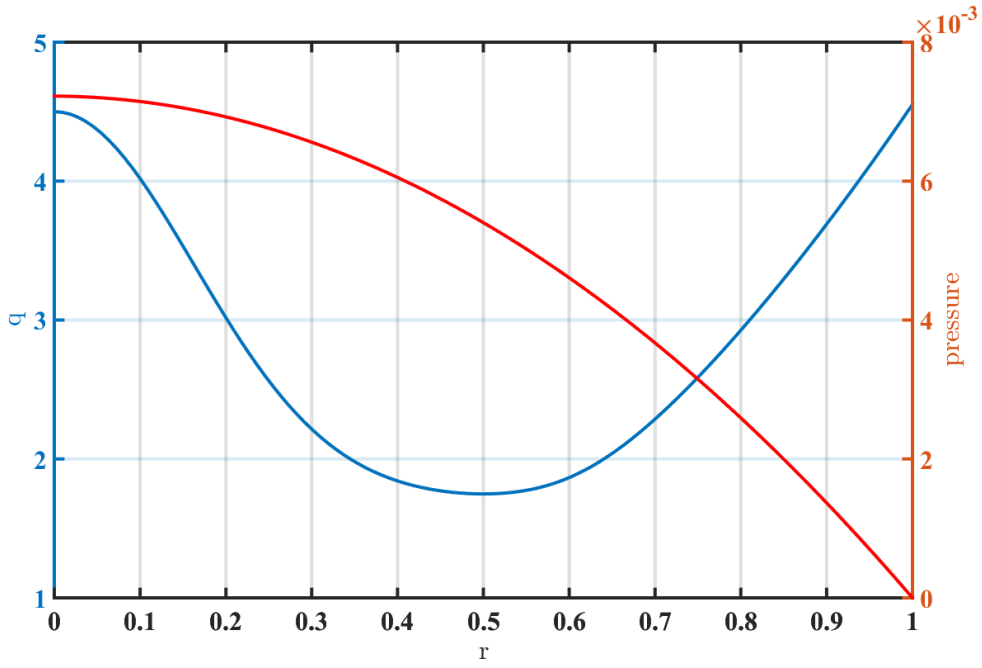

Figure 1 Initial safety factor and plasma pressure profiles.

In the system, the most unstable mode is the m/n=2/1 DTM. The initial equilibrium is derived from the QSOLVER code.[44] The normalized parameters are chosen to be $\eta = 1.0\times10^{-6}$, $\nu = 1\times10^{-5}$, $\kappa_{\perp} = 5\times10^{-6}$, $\kappa_{\parallel} = 1.0$, and $D = 1\times10^{-4}$. The grids used in simulations are $256\times32\times256\,(R,\varphi,Z)$, and the convergence study has

been ensured by using grids $400\times64\times400\ (R,\varphi,Z)$.

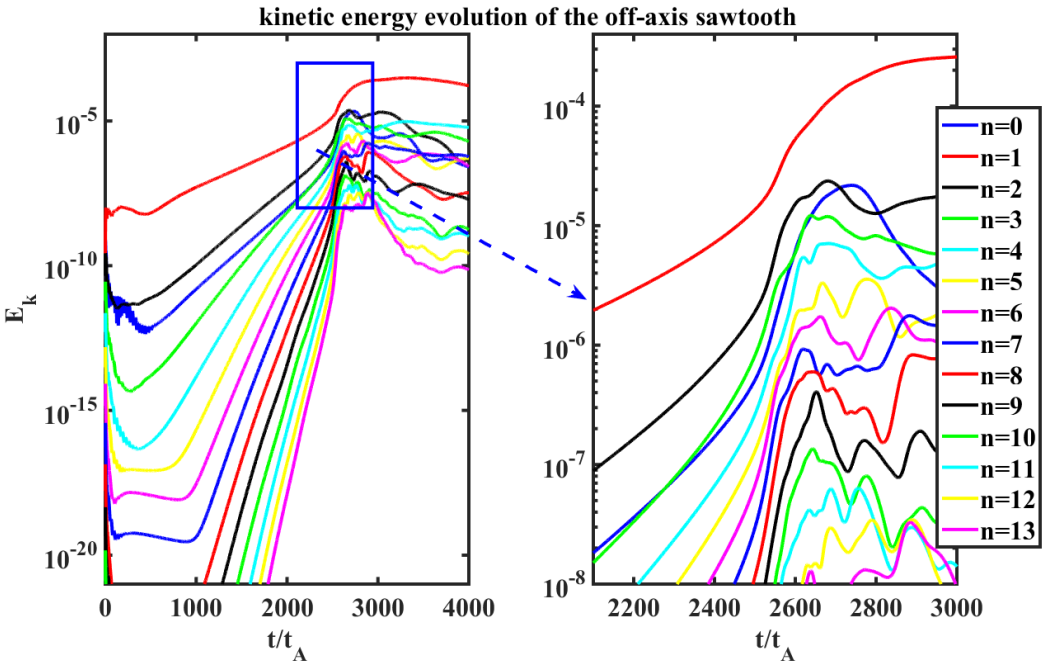

Figure 2 The evolution of the kinetic energy for different toroidal mode numbers in the off-axis crash sawtooth. At about $t=2500t_A$, the modes begin to abrupt.

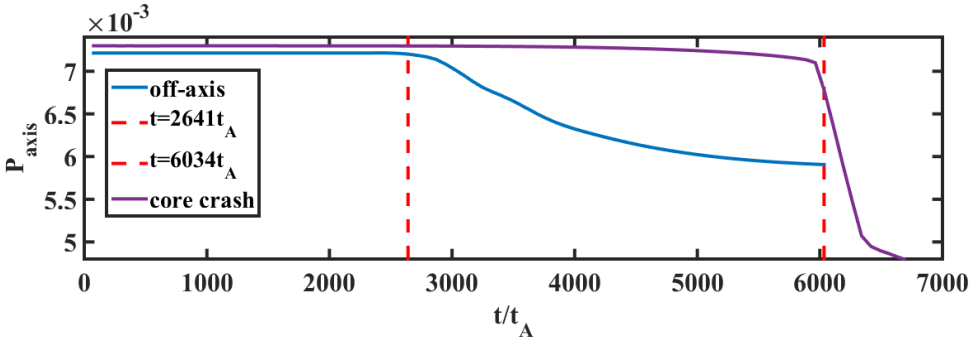

Figure 3 Evolutions of the plasma pressure at the magnetic axis P_{axis}. The time scale of the pressure crash for the off-axis crash sawtooth is over $3000\,t_A$ that is much longer than that for the core-crash sawtooth.

The evolution of the kinetic energy for different toroidal mode numbers for the off-axis crash sawtooth is shown in Figure 2. At the nonlinear stage, magnetic reconnection exhibits substantial enhancement, and all modes experience explosive

growth due to the nonlinear mode-mode coupling effect, which is similar to the core-crash sawtooth.[43] However, from the time evolutions of the plasma pressure at the magnetic axis for the off-axis pressure crash and the core pressure crash, as shown in Figure 3, it is evident that the time scale of the pressure crash for the off-axis pressure crash is over $3000t_A$, which is much longer than that in the core crash sawtooth. For typical TFTR parameters, the time scale in the off-axis crash is about $320\mu s$, while the time scale of the pressure crash during the core crash is only 20~40 μs.[38]

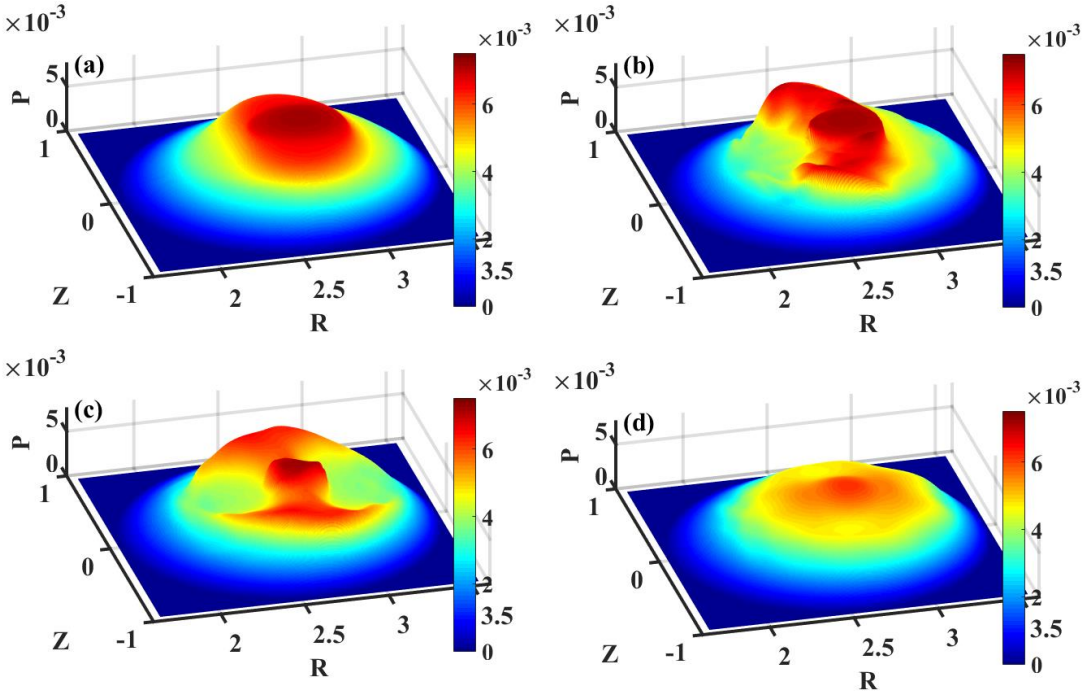

Figure 4 The color isosurface plots of the plasma pressure at four typical moments: (a) $t = 2414t_A$ at the m/n=2/1 DTM precursor, (b) $t = 2641t_A$ at the beginning, (c) $t = 2942t_A$ at the end, and (d) $t = 4526t_A$ at the final state of the pressure crash.

The color isosurface plots of the plasma pressure at four typical moments (a) $t = 2414t_A$ at the m/n=2/1 DTM precursor, (b) $t = 2641t_A$ at the beginning, (c) $t = 2942t_A$ at the end, and (d) $t = 4526t_A$ at the final state of the pressure crash are shown in Figure 4. The hot plasma in the core region gradually becomes an ellipse

before the crash (Figure 4a). During the crash, the plasma pressure around the magnetic axis keeps almost unchanged, and the pressure crash only occurs annular region (Figure 4b and 4c), which is the reason why it is called an off-axis crash. The pressure evolution is well consistent with experimental observations (Figure 2a in Ref.[38]). As shown in Figure 4d, the plasma pressure at the magnetic axis will slowly decrease, and the pressure profiles become flattened in the whole core region, which is also consistent with TFTR observations (Figure 1c in Ref.[38]).

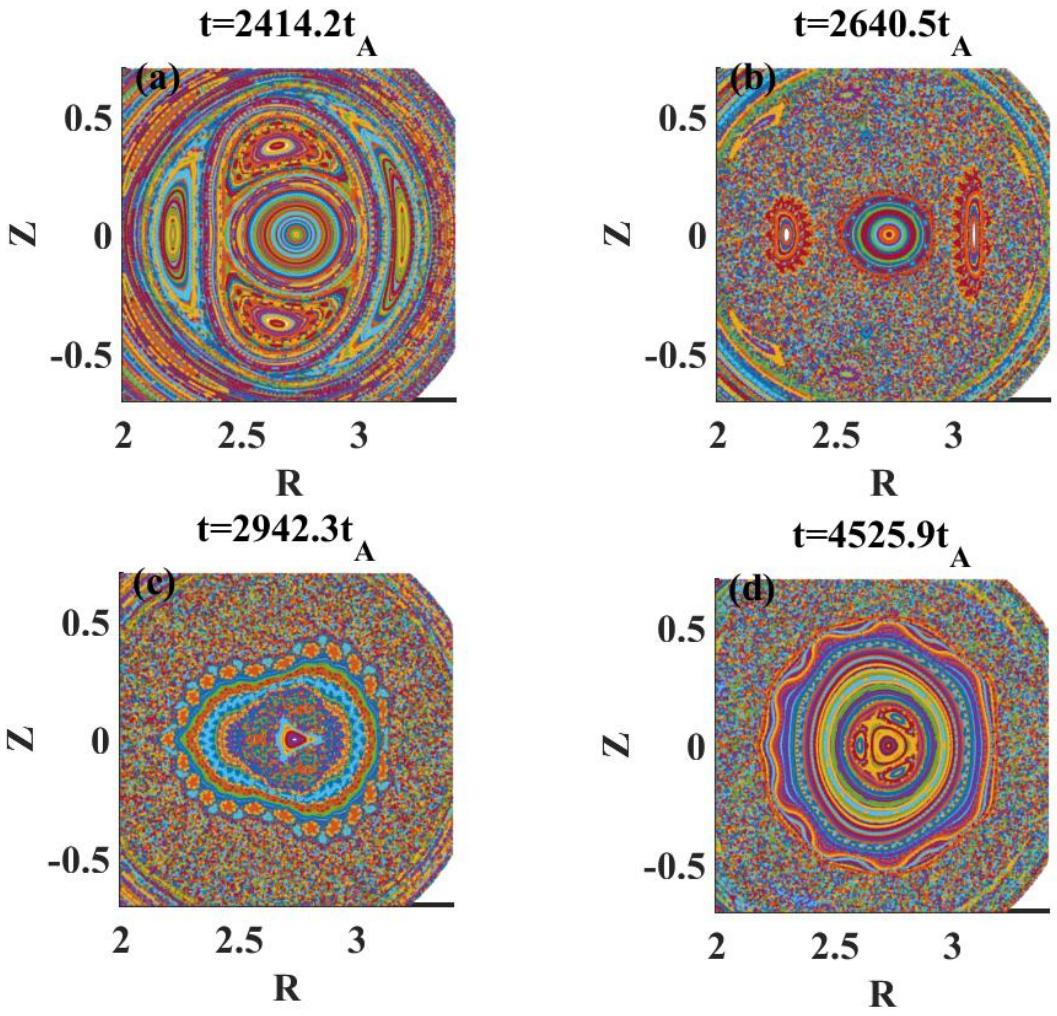

Figure 5 The Poincare plots of the plasma pressure at the same four moments as in Figure 4: (a) $t = 2414t_A$ at the m/n=2/1 DTM precursor, (b) $t = 2641t_A$ at the begin, (c) $t = 2942t_A$ at the end, and (d) $t = 4526t_A$ at the final state of the pressure crash.

The Poincare plots at the same moments with that in Figure 4 are shown in Figure

5. At $t = 2414t_A$, two pairs of the m/n=2/1 magnetic islands form in the inner and outer $q = 2$ resonant surfaces. Due to the development of the m/n=2/1 DTM and the large parallel thermal conductivity, the plasma pressure becomes flattened inside the islands. As a result, an ellipse like hot plasma region is formed during the DTM precursor (Figure 4a). At the nonlinear stage, the outer two m/n=2/1 islands gradually expand inwards while the inner two islands are squeezed outwards (Figure 5b), which is similar to that in the core pressure crash. However, it should be noted that the magnetic flux surfaces around the magnetic axis have not been destroyed during the off-axis crash (Figure 5c and 5d), which is significantly different from that in the core pressure crash. That is the reason why the plasma pressure around the magnetic axis only has a small change during the crash.

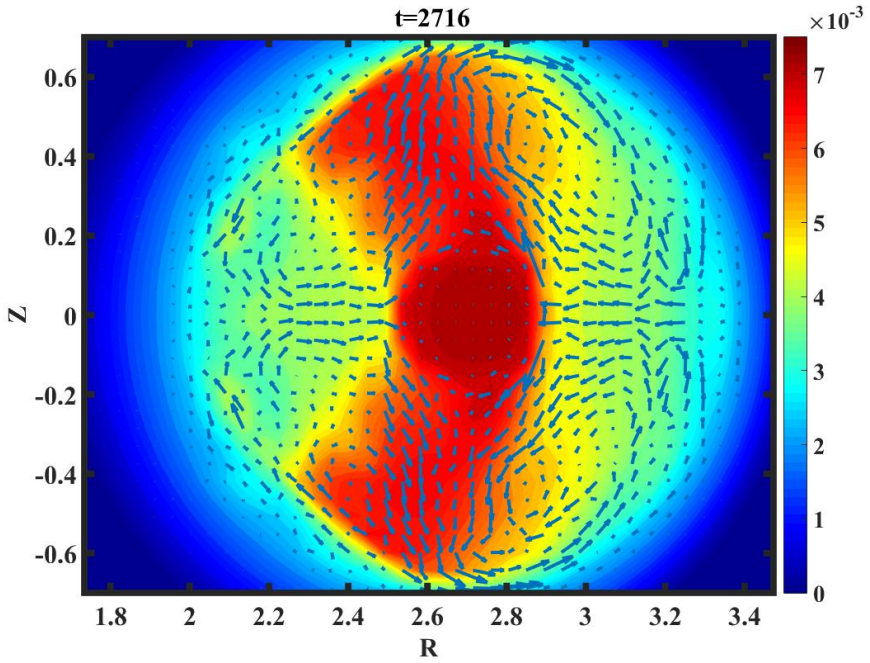

Figure 6 Flow patterns at $t = 2716t_A$. It should be noted that the flow near the magnetic axis is weak, and the strong plasma flows in other regions detour around the magnetic axis.

The flow patterns at $t = 2716t_A$ (in the middle of the crash) are shown in Figure 6. It is clear that the strong plasma flow resulted from the burst of magnetic reconnection is blocked by undestroyed magnetic surfaces and detours around the

magnetic axis. Hence, the plasma flow near the magnetic axis is very weak, which leads to that the pressure at the magnetic axis has a slight decrease during the off-axis crash.

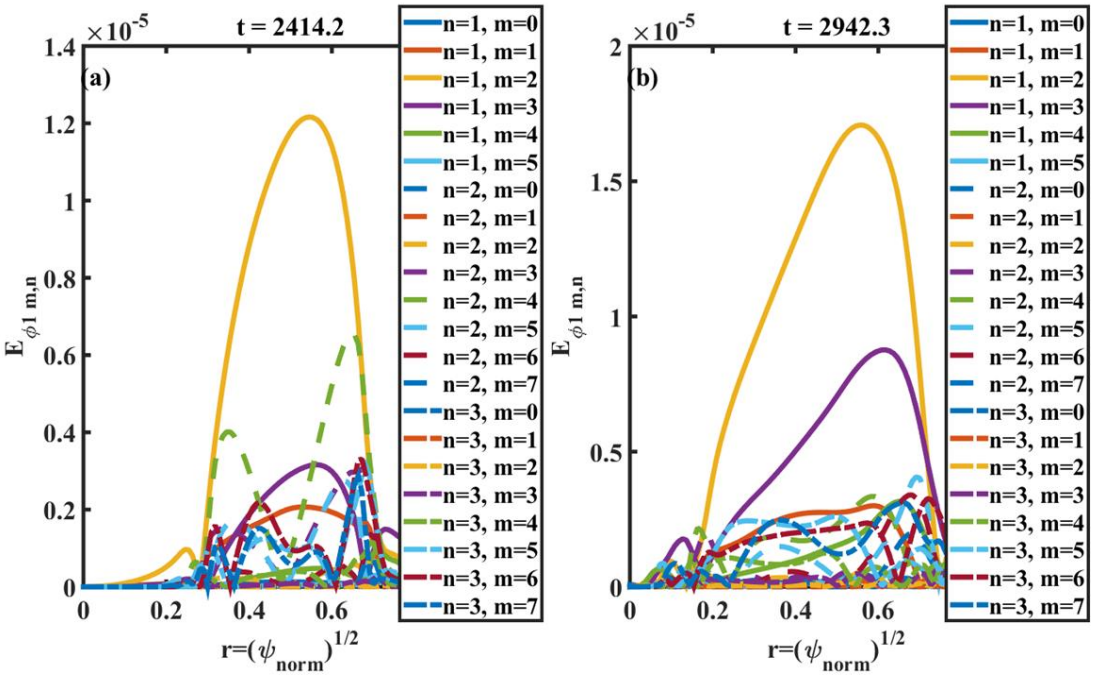

Figure 7 The mode structures at (a) $t = 2414t_A$ before the crash and (b) $t = 2716t_A$ at the end of the crash.

The mode structures (a) $t = 2414t_A$ before the crash and (b) $t = 2716t_A$ at the end of the crash are shown in Figure 7. Although the mode structure of the m/n=2/1 DTM has a significant expansion during the crash, it remains very small in the vicinity of the magnetic axis, which is quite different from the core pressure crash. Since the modes never reach the region around the magnetic axis, the on-axis pressure will not be affected by the DTM, and keeps almost unchanged during the crash.

B. The transition condition between the off-axis and core pressure crash

As shown in Section III.A, the nonlinear evolution of the m/n=2/1 DTM could result in the off-axis crash in some cases, but in other cases could lead to the core pressure crash. [43] Also, in TFTR observations[38], both kinds of pressure crash were reported to be related to the nonlinear evolution of the m/n=2/1 DTM. However,

the transition between the two different kinds of pressure crashes has not been clearly understood.

From a theoretical point of view, the destruction of the magnetic surfaces should always be related to the reconnection process. For the off-axis pressure crash, the magnetic surfaces in the vicinity of the magnetic axis should not be destroyed, which means there should be notable poloidal magnetic flux left after the pressure crash; for the cases with the core pressure crash, the magnetic surfaces around the magnetic axis are totally destroyed, which means that all the poloidal flux inside the inner q=2 surfaces are reconnected during the crash. As a result, the two resonant surfaces' radial locations should significantly influence the type of crashes since it determines the total poloidal flux inside the inner q=2 resonant surface ($\psi_1 = r_1^2$) and the poloidal flux inside the two resonant surfaces ($\Delta\psi = \psi_2 - \psi_1 = r_2^2 - r_1^2$). The reconnection rate on the two resonant surfaces should depend on the magnetic shear on the two resonant surfaces (s_1 and s_2). Hence, the transition criterion should be that all poloidal flux inside the inner q=2 surface is completely reconnected out at the end of the pressure crash.

$$\frac{\psi_1}{|s_1|} \simeq \frac{\psi_2 - \psi_1}{|s_1| + s_2} \tag{9}$$

Or

$$\frac{r_1^2}{|s_1|} \simeq \frac{r_2^2 - r_1^2}{|s_1| + s_2} \tag{10}$$

Therefore, the criterion for the off-axis pressure crash is

$$r_1 > \sqrt{\frac{|s_1|}{2|s_1| + s_2}}\, r_2 . \tag{11}$$

For the q profile used in Section III.A, we have $r_1 = 0.35, r_2 = 0.6, s_1 = -0.64$, and $s_2 = 1.29$, thus the criterion for the off-axis pressure is satisfied, i.e., $r_1 = 0.35 > \sqrt{\frac{|s_1|}{2|s_1| + s_2}}\, r_2 = 0.31$. It is why the DTM leads to the off-axis pressure crash instead of the core pressure crash in the previous subsection.

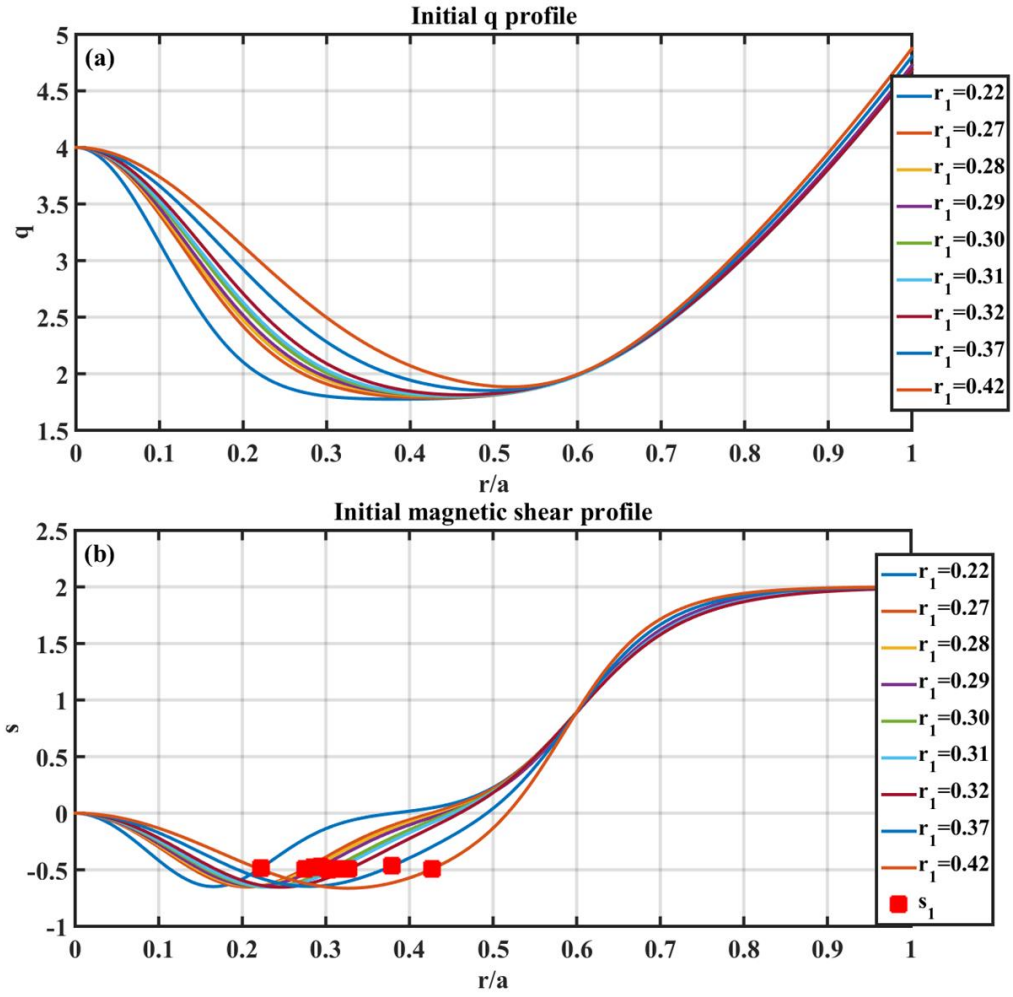

Figure 8 The initial q and magnetic shear profiles with different r_1 and fixed $r_2 = 0.6$, $s_1 \sim -0.49$, and $s_2 \sim 0.91$. The parameters used for generating the initial equilibriums with $r_2 = 0.6$, $s_1 \sim -0.49$, $s_2 \sim 0.91$, and different r_1 are given in Table 1 of the Appendix.

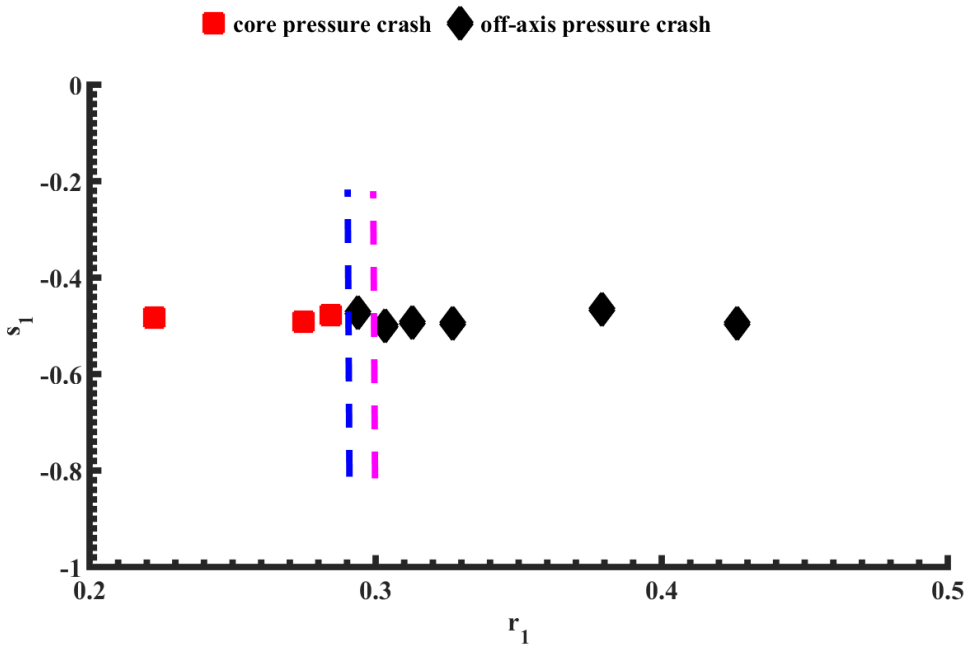

Figure 9 The nonlinear behavior of the m/n=2/1 DTM with different r_1. If $r_1 < 0.29$, the nonlinear evolution of DTM will lead to the core pressure crash; otherwise, it results in the off-axis pressure crash. The transition criteria of r_1 are indicated by the blue dash line (for the simulations) and the pink dash line (for the simple model, i. e. Eq. (11)), respectively.

A series of systematical simulations are carried out to examine the transition criterion between the core and off-axis pressure crashes given by Eq. (11). Firstly, the influence of the radial location of the inner resonant surface r_1 is investigated. The initial q profiles and the magnetic shear profiles based on Equation (7) are shown in Figure 8. In these initial equilibria, we choose different r_1 and keep the other three parameters r_2, s_1, and s_2 fixed (where r_2 is the radial position of the outer resonant surface, s_1, and s_2 are the magnetic shear at the inner and outer resonant surfaces, respectively). As shown in Figure 9, the larger r_1, it is more likely that DTM leads to the off-axis pressure crash. The transition criterion is about $r_1 = 0.29$. Below this value, the nonlinear evolution of the m/n=2/1 DTM will finally result in the core pressure crash. Otherwise, it will lead to the off-axis pressure crash. The

transition criterion from Equation (11) is $r_1 \sim 0.30$ that agrees well with that from our simulations.

Since the local magnetic shear s_1 determines the reconnection rate at the inner resonant surface, we have also studied its influence. The initial q profiles with different s_1 are shown in Figure 10(a) r_1=0.27, 10(b) r_1=0.29, and 10(c) r_1=0.33. In these initial equilibriums, s_2 and r_2 are kept unchanged. As shown in Figure 11, for the fixed r_1, the smaller $|s_1|$, the slower reconnection at the inner resonant surface, the more magnetic flux left inside the inner resonant surface, and the more likely that the DTM results in the off-axis pressure crash. As a result, the critical $|s_1|$ decreases with increasing r_1 for the two different kinds of nonlinear DTM evolutions. For r_1=0.27, the transition criterion is $|s_1| \sim 0.4$, and for r_1=0.29, it is $|s_1| \sim 0.67$. From Equation (11), we can also derive the transition criterion for s_1,

$$|s_1| = \frac{s_2 r_1^2}{r_2^2 - 2r_1^2} \tag{12}$$

With r_1=0.27, the transition criterion is $|s_1| \sim 0.33$, which is a little different from the simulations ($|s_1| \sim 0.40$). With r_1=0.29, the transition criterion from Equation (12) gives $|s_1| \sim 0.45$, which is different from the simulations ($|s_1| \sim 0.67$). In the simulations with $r_1 = 0.33$, the nonlinear DTM evolutions all result in the off-axis pressure crash since the magnetic flux inside the inner resonant surface is abundant. However, the transition condition derived from Equation (12) is about $|s_1| \sim 0.70$.

The transition criterion's tendencies from the simulations and Equation (12) are qualitatively the same, but quantitatively different. The quantitative difference between the transition criteria from the simulations and Equation (12) indicates that the dependence of the transition criterion on the magnetic shear is more complicated than Equation (9).

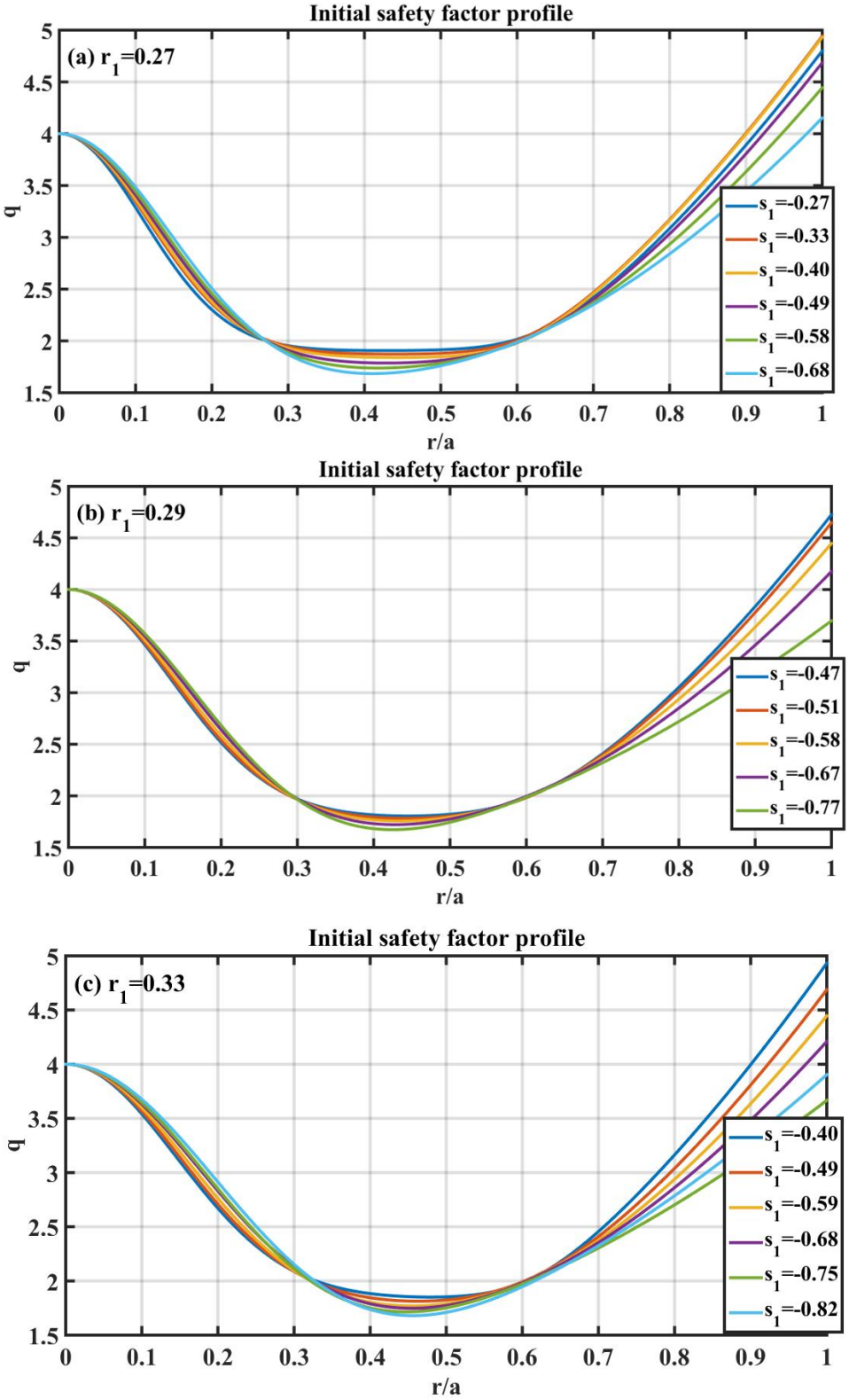

Figure 10 The initial q profiles with different magnetic shears at the inner resonant surface (a) r_1=0.27 , (b) r_1=0.29 , and (c) r_1=0.33 . The parameters used for generating the initial equilibriums with (a) $r_2 = 0.6$, $r_1 \sim 0.27$, $s_2 \sim 0.91$, and different s_1, (b) $r_2 = 0.6$, $r_1 \sim 0.29$, $s_2 \sim 0.91$, and different s_1, and (c) $r_2 = 0.6$,

$r_1 \sim 0.33$, $s_2 \sim 0.91$, and different s_1 are given in Table 2, 3 ,and 4 of the Appendix, respectively.

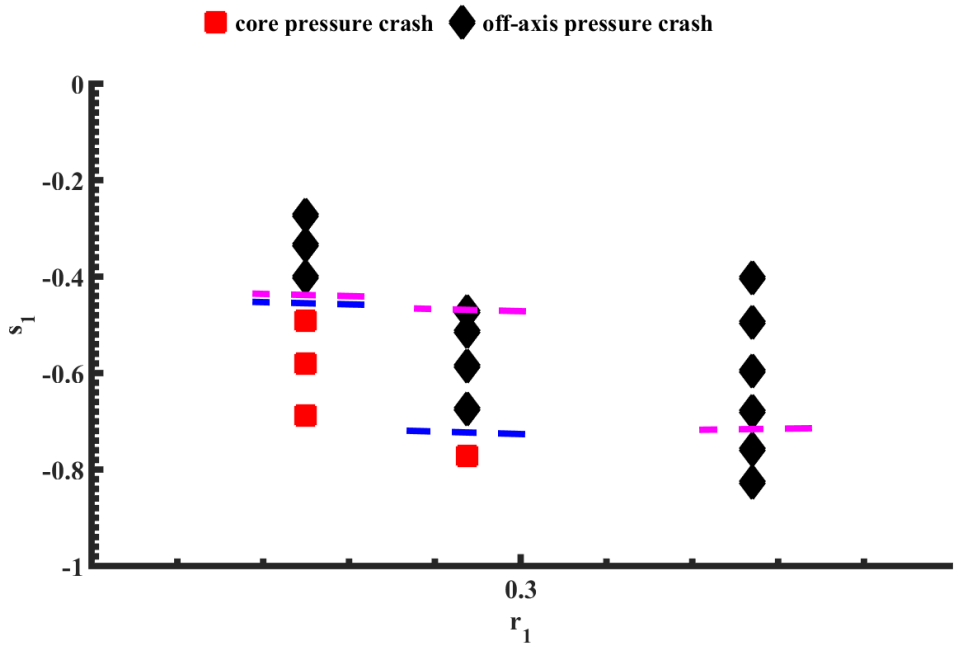

Figure 11 The nonlinear behaviors of the DTM with different r_1 and s_1. The transition criteria are indicated by the blue dash line (for the simulations) and the pink dash line (for the simple model, i. e. Eq. (12)), respectively.

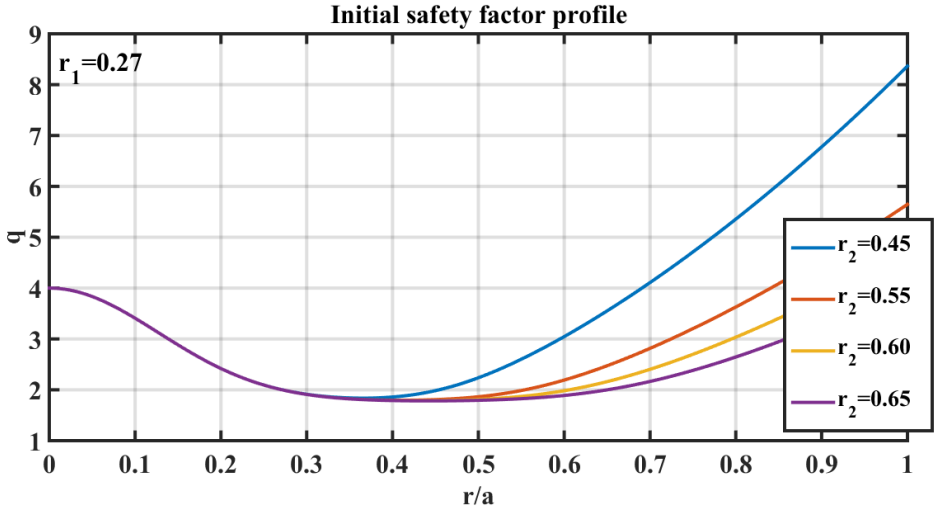

Figure 12 The initial q profiles with different r_2 and fixed r_1=0.27 . The parameters used for generating the initial equilibriums with $r_1 \sim 0.27$, $s_1 \sim -0.49$,

$s_2 \sim 0.91$, and different r_2 are given in Table 5 of the Appendix.

The influence of the spatial separation between the two resonant surfaces are also investigated. The initial q profiles with different r_2 and fixed r_1=0.27 are shown in Figure 12. As shown in Figure 13, for the cases with r_1=0.27 and r_2=0.60 or r_2=0.65, the nonlinear DTM evolution causes the core pressure crash. While with smaller separation (i.e., r_2=0.45 or r_2=0.55), the nonlinear DTM leads to the off-axis pressure crash. It is because that the larger spatial separation between the two resonant will leave more space for the DTM to develop, finally the less flux left inside the inner resonant surface, and then it is more likely to lead to the core pressure crash. From Eq. (11), we have the transition criterion for r_2,

$$r_2 > \sqrt{\frac{2|s_1|+s_2}{|s_1|}}\, r_1 . \tag{13}$$

With $r_1 \sim 0.27$, $s_1 \sim -0.49$, $s_2 \sim 0.91$, the transition criterion of the outer resonant surface position should be r_2=0.54, which is in good agreement with that from the simulations.

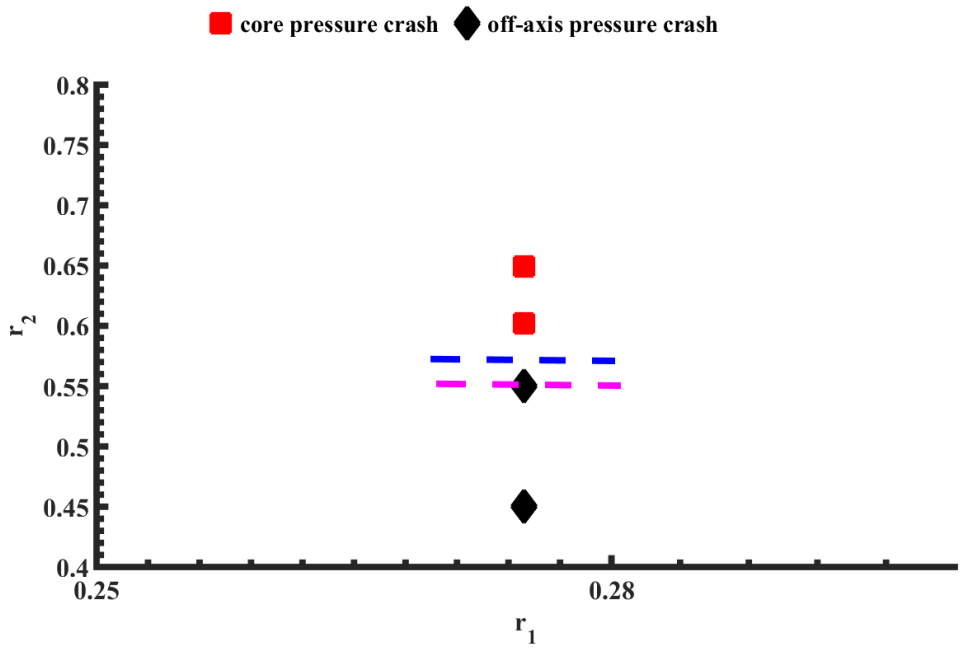

Figure 13 The nonlinear behaviors of the DTM with different r_2. The transition criteria for the outer resonant surface position are indicated by the blue dash line from simulations and the pink dash line from Equation (12), respectively.

IV. Discussion and conclusion

The off-axis pressure crash resulted from the nonlinear evolution of the m/n=2/1 DTM is investigated. During the off-axis pressure crash, the plasma pressure at the magnetic axis keeps almost unchanged, and the crash only occurs in the annular region; after the crash, the plasma pressure slowly reduces, which is well consistent with TFTR observations.[38]

The magnetic flux surfaces in the vicinity of the magnetic axis remain almost unchanged during the crash, which is why the pressure around the magnetic axis decreases very slowly. The flow patterns and the mode structure also indicate that there is no plasma flow and the magnetic surfaces are undestroyed in the core region around the magnetic axis until the end of the m/n=2/1 DTM, and strong dynamic process only takes place in the annular region.

A series of simulations are carried out to investigate the influence of the radial position of the inner resonant surface r_1 (or the normalized magnetic flux inside the

inner resonant surface since $\psi_1 = r_1^2$), the magnetic shear at the inner resonance surface s_1, and the radial position of the outer resonant surface r_2. We find that r_1 is the dominant factor for the two kinds of behaviors of the DTM. For a smaller r_1, the magnetic flux inside the inner resonant surface is less, and then the DTM leads to a core-crash sawtooth and vice versa. Since the magnetic shear at the inner resonant surface determines the local reconnection rate, it can also influence the critical r_1. With larger $|s_1|$, the magnetic reconnection at the inner resonant surface is faster. As a result, the critical r_1 increases with increasing $|s_1|$. The spatial separation between the two q=2 resonant surfaces can also influence the critical r_1 since the larger separation, the more space for the development of the DTM, and the more likely to lead to a core-crash sawtooth. A simple theoretical formula of the transition criterion is proposed, which is in good agreement with the simulation results.

Appendix

In the appendix, the detailed parameters for different initial profiles are presented.

	q_0	r_0	λ	A	δ
$r_1 = 0.22$	4.0	0.615	5.08	1.26	0.145
$r_1 = 0.27$	4.0	0.615	5.08	1.26	0.180
$r_1 = 0.28$	4.0	0.615	5.43	1.24	0.185
$r_1 = 0.29$	4.0	0.615	5.43	1.24	0.190
$r_1 = 0.30$	4.0	0.615	5.08	1.26	0.200
$r_1 = 0.31$	4.0	0.615	5.08	1.26	0.205
$r_1 = 0.32$	4.0	0.615	4.93	1.26	0.215
$r_1 = 0.37$	4.0	0.61	5.73	1.24	0.245

$r_1 = 0.42$	4.0	0.60	6.13	1.28	0.285

Table 1 The parameters used for generating the initial equilibriums with $r_2 = 0.6$, $s_1 \sim -0.49$, $s_2 \sim 0.91$, and different r_1.

	q_0	r_0	λ	A	δ
$s_1 = -0.27$	4.0	0.630	7.13	1.10	0.155
$s_1 = -0.33$	4.0	0.615	7.38	1.14	0.165
$s_1 = -0.40$	4.0	0.610	7.43	1.18	0.170
$s_1 = -0.49$	4.0	0.615	5.08	1.26	0.180
$s_1 = -0.58$	4.0	0.620	3.68	1.36	0.190
$s_1 = -0.68$	4.0	0.625	2.48	1.56	0.205

Table 2 The parameters used for generating the initial equilibriums with $r_2 = 0.6$, $r_1 \sim 0.27$, $s_2 \sim 0.91$, and different s_1.

	q_0	r_0	λ	A	δ
$s_1 = -0.47$	4.0	0.615	5.43	1.24	0.190
$s_1 = -0.51$	4.0	0.615	4.78	1.28	0.195
$s_1 = -0.58$	4.0	0.620	3.63	1.36	0.205
$s_1 = -0.67$	4.0	0.625	2.53	1.54	0.220
$s_1 = -0.77$	4.0	0.630	1.13	2.56	0.235

Table 3 The parameters used for generating the initial equilibriums with $r_2 = 0.6$, $r_1 \sim 0.29$, $s_2 \sim 0.91$, and different s_1.

	q_0	r_0	λ	A	δ
$s_1 = -0.40$	4.0	0.610	7.43	1.18	0.205
$s_1 = -0.49$	4.0	0.615	4.93	1.26	0.215
$s_1 = -0.59$	4.0	0.615	3.53	1.40	0.230
$s_1 = -0.68$	4.0	0.610	2.48	1.64	0.250
$s_1 = -0.75$	4.0	0.610	1.01	3.0	0.250
$s_1 = -0.82$	4.0	0.510	1.01	3.94	0.255

Table 4 The parameters used for generating the initial equilibriums with $r_2 = 0.6$, $r_1 \sim 0.33$, $s_2 \sim 0.91$, and different s_1.

$r_1 = 0.27$	q_0	r_0	λ	A	δ
$r_2 = 0.45$	4.0	0.460	5.23	1.26	0.180
$r_2 = 0.55$	4.0	0.560	5.23	1.26	0.180
$r_2 = 0.60$	4.0	0.615	5.08	1.26	0.180
$r_2 = 0.65$	4.0	0.665	4.83	1.26	0.180

Table 5 The parameters used for generating the initial equilibriums with $r_1 \sim 0.27$, $s_1 \sim -0.49$, $s_2 \sim 0.91$, and different r_2.

Acknowledgment

This work is supported by the National Natural Science Foundation of China under Grant No. 11775188 and 11835010, the Special Project on High-performance Computing under the National Key R&D Program of China No. 2016YFB0200603, Fundamental Research Fund for Chinese Central Universities.

Reference

[1] C. Kessel, J. Manickam, G. Rewoldt, W.M. Tang, Improved plasma performance in tokamaks with negative magnetic shear, Physical Review Letters, 72 (1994) 1212-1215.
[2] A. Sykes, J.A. Wesson, S.J. Cox, High-$\ensuremath{\beta}$ Tokamaks, Physical Review Letters, 39 (1977) 757-760.
[3] H.Y. Yuh, S.M. Kaye, F.M. Levinton, E. Mazzucato, D.R. Mikkelsen, D.R. Smith, R.E. Bell, J.C. Hosea, B.P. LeBlanc, J.L. Peterson, H.K. Park, W. Lee, Suppression of Electron Temperature Gradient Turbulence via Negative Magnetic Shear in NSTX, Physical Review Letters, 106 (2011) 055003.
[4] J.W. Connor, T. Fukuda, X. Garbet, C. Gormezano, V. Mukhovatov, M. Wakatani, t.I.T.B.D. Group, t.I.T.G.o. Transport, I.B. Physics, A review of internal transport barrier physics for steady-state operation of tokamaks, Nuclear Fusion, 44 (2004) R1-R49.
[5] T. Fujita, S. Ide, H. Shirai, M. Kikuchi, O. Naito, Y. Koide, S. Takeji, H. Kubo, S. Ishida, Internal Transport Barrier for Electrons in JT-60U Reversed Shear Discharges, Physical Review Letters, 78 (1997) 2377-2380.
[6] R.C. Wolf, Internal transport barriers in tokamak plasmas*, Plasma Physics and Controlled Fusion, 45 (2002) R1-R91.
[7] E.J. Strait, L.L. Lao, M.E. Mauel, B.W. Rice, T.S. Taylor, K.H. Burrell, M.S. Chu, E.A. Lazarus, T.H. Osborne, S.J. Thompson, A.D. Turnbull, Enhanced Confinement and Stability in DIII-D Discharges with Reversed Magnetic Shear, Physical Review Letters, 75 (1995) 4421-4424.
[8] E. Joffrin, C.D. Challis, G.D. Conway, X. Garbet, A. Gude, S. Günter, N.C. Hawkes, T.C. Hender, D.F. Howell, G.T.A. Huysmans, E. Lazzaro, P. Maget, M. Marachek, A.G. Peeters, S.D. Pinches, S.E. Sharapov, J.-E. contributors, Internal transport barrier triggering by rational magnetic flux surfaces in tokamaks, Nuclear Fusion, 43 (2003) 1167-1174.
[9] F.M. Levinton, M.C. Zarnstorff, S.H. Batha, M. Bell, R.E. Bell, R.V. Budny, C. Bush, Z. Chang, E. Fredrickson, A. Janos, J. Manickam, A. Ramsey, S.A. Sabbagh, G.L. Schmidt, E.J. Synakowski, G. Taylor, Improved Confinement with Reversed Magnetic Shear in TFTR, Physical Review Letters, 75 (1995) 4417-4420.
[10] Y.X. Wan, J.G. Li, Y. Liu, X.L. Wang, C. Vincent, C.G. Chen, X.R. Duan, P. Fu, X. Gao, K.M. Feng, S.l. Liu, Y.T. Song, P.D. Weng, B.N. Wan, F.R. Wan, H.Y. Wang, S.T. Wu, M.Y. Ye, Q.W. Yang, G.Y. Zheng, G. Zhuang, Q. Li, C. team, Overview of the present progress and activities on the CFETR, Nuclear Fusion, 57 (2017) 102009.
[11] A.C.C. Sips, f.t.S.S. Operation, t.T.P.t.g. Activity, Advanced scenarios for ITER Plasma Physics and Controlled Fusion, 47 (2005) A19-A40.
[12] B. Carreras, H.R. Hicks, B.V. Waddell, Tearing-mode activity for hollow current profiles, Nuclear Fusion, 19 (1979) 583.
[13] P.L. Pritchett, Y.C. Lee, J.F. Drake, Linear analysis of the double-tearing mode, The Physics of Fluids, 23 (1980) 1368-1374.
[14] J.W. Connor, S.C. Cowley, R.J. Hastie, T.C. Hender, A. Hood, T.J. Martin, Tearing modes in toroidal geometry, The Physics of Fluids, 31 (1988) 577-590.

[15] Q. Yu, S. Günter, Numerical modelling of neoclassical double tearing modes, Nuclear Fusion, 39 (1999) 487.
[16] Y. Ishii, M. Azumi, G. Kurita, T. Tuda, Nonlinear evolution of double tearing modes, Physics of Plasmas, 7 (2000) 4477-4491.
[17] E. Fredrickson, M. Bell, R.V. Budny, E. Synakowski, Nonlinear evolution of double tearing modes in tokamaks, Physics of Plasmas, 7 (2000) 4112-4120.
[18] M. Taro, N. Hiroshi, T. Shinji, K. Yasuaki, Nonlinear behaviour of collisionless double tearing mode induced by electron inertia, Nuclear Fusion, 45 (2005) 1264.
[19] A. Bierwage, S. Hamaguchi, M. Wakatani, S. Benkadda, X. Leoncini, Nonlinear Evolution of $q=1$ Triple Tearing Modes in a Tokamak Plasma, Physical Review Letters, 94 (2005) 065001.
[20] A. Bierwage, M. Toma, K. Shinohara, MHD and resonant instabilities in JT-60SA during current ramp-up with off-axis N-NB injection, Plasma Physics and Controlled Fusion, 59 (2017) 125008.
[21] Z.X. Wang, X.G. Wang, J.Q. Dong, Y.A. Lei, Y.X. Long, Z.Z. Mou, W.X. Qu, Fast Resistive Reconnection Regime in the Nonlinear Evolution of Double Tearing Modes, Physical Review Letters, 99 (2007) 185004.
[22] M. Janvier, Y. Kishimoto, J. Li, Critical parameters for the nonlinear destabilization of double tearing modes in reversed shear plasmas, Nuclear Fusion, 51 (2011) 083016.
[23] M. Janvier, Y. Kishimoto, J.Q. Li, Structure-Driven Nonlinear Instability as the Origin of the Explosive Reconnection Dynamics in Resistive Double Tearing Modes, Physical Review Letters, 107 (2011) 195001.
[24] A. Mao, J. Li, J. Liu, Y. Kishimoto, Zonal flow dynamics in the double tearing mode with antisymmetric shear flows, Physics of Plasmas, 21 (2014) 052304.
[25] A. Mao, J. Li, Y. Kishimoto, J. Liu, Eigenmode characteristics of the double tearing mode in the presence of shear flows, Physics of Plasmas, 20 (2013) 022114.
[26] Z.-X. Wang, L. Wei, X. Wang, The q-profile effect on high-order harmonic q = 1 tearing mode generation during sawtooth crashes, Physics of Plasmas, 19 (2012) 062108.
[27] J. Wang, Z.X. Wang, L. Wei, Y. Liu, Control of neo-classical double tearing modes by differential poloidal rotation in reversed magnetic shear tokamak plasmas, Nuclear Fusion, 57 (2017) 046007.
[28] Z.-X. Wang, L. Wei, F. Yu, Nonlinear evolution of neo-classical tearing modes in reversed magnetic shear tokamak plasmas, Nuclear Fusion, 55 (2015) 043005.
[29] A. Ali, J. Li, Y. Kishimoto, On the abrupt growth dynamics of nonlinear resistive tearing mode and the viscosity effects, Physics of Plasmas, 21 (2014) 052312.
[30] J. Pétri, M. Takamoto, H. Baty, S. Zenitani, Explosive reconnection of the double tearing mode in relativistic plasmas with application to the Crab nebula, Plasma Physics and Controlled Fusion, 57 (2014) 014034.
[31] A. Mao, J. Li, J. Liu, Y. Kishimoto, Nonlinear evolution of the Kelvin-Helmholtz instability in the double current sheet configuration, Physics of Plasmas, 23 (2016) 032117.
[32] T. Akramov, H. Baty, Non-linear growth of double tearing mode: Explosive

reconnection, plasmoid formation, and particle acceleration, Physics of Plasmas, 24 (2017) 082116.
[33] W. Guo, J. Ma, Q. Yu, Numerical study on nonlinear growth of m/n = 3/1 double tearing mode in high Lundquist number regime, Plasma Physics and Controlled Fusion, 61 (2019) 075011.
[34] J. Ma, W. Guo, Z. Yu, Q. Yu, Effect of plasmoids on nonlinear evolution of double tearing modes, Nuclear Fusion, 57 (2017) 126004.
[35] T. Liu, Z.X. Wang, J.L. Wang, L. Wei, Suppression of explosive bursts triggered by neo-classical tearing mode in reversed magnetic shear tokamak plasmas via ECCD, Nuclear Fusion, 58 (2018) 076026.
[36] W. Tang, Z.-X. Wang, L. Wei, J. Wang, S. Lu, Control of neoclassical tearing mode by synergetic effects of resonant magnetic perturbation and electron cyclotron current drive in reversed magnetic shear tokamak plasmas, Nuclear Fusion, 60 (2020) 026015.
[37] C.L. Zhang, Z.W. Ma, Nonlinear evolution of double tearing mode in Hall magnetohydrodynamics, Physics of Plasmas, 16 (2009) 122113.
[38] Z. Chang, W. Park, E.D. Fredrickson, S.H. Batha, M.G. Bell, R. Bell, R.V. Budny, C.E. Bush, A. Janos, F.M. Levinton, K.M. McGuire, H. Park, S.A. Sabbagh, G.L. Schmidt, S.D. Scott, E.J. Synakowski, H. Takahashi, G. Taylor, M.C. Zarnstorff, Off-Axis Sawteeth and Double-Tearing Reconnection in Reversed Magnetic Shear Plasmas in TFTR, Physical Review Letters, 77 (1996) 3553-3556.
[39] M.R. de Baar, G.M.D. Hogeweij, N.J. Lopes Cardozo, A.A.M. Oomens, F.C. Schüller, Electron Thermal Transport Barrier and Magnetohydrodynamic Activity Observed in Tokamak Plasmas with Negative Central Shear, Physical Review Letters, 78 (1997) 4573-4576.
[40] S. Günter, S. Schade, M. Maraschek, S.D. Pinches, E. Strumberger, R. Wolf, Q. Yu, A.U. Team, MHD phenomena in reversed shear discharges on ASDEX Upgrade, Nuclear Fusion, 40 (2000) 1541.
[41] M. Xu, H.L. Zhao, Q. Zang, G.Q. Zhong, L.Q. Xu, H.Q. Liu, W. Chen, J. Huang, L.Q. Hu, G.S. Xu, X.Z. Gong, J.P. Qian, Y. Liu, T. Zhang, Y. Zhang, Y.W. Sun, X.D. Zhang, B.N. Wan, Characteristics of off-axis sawteeth with an internal transport barrier in EAST, Nuclear Fusion, 59 (2019) 084005.
[42] Y. Ishii, M. Azumi, Y. Kishimoto, J.N. Leboeuf, Long timescale plasma dynamics and explosive growth driven by the double tearing mode in reversed shear plasmas, Nuclear Fusion, 43 (2003) 539.
[43] W. Zhang, Z.W. Ma, J. Zhu, H.W. Zhang, Core-crash sawtooth associated with m/n = 2/1 double tearing mode in Tokamak, Plasma Physics and Controlled Fusion, 61 (2019) 075002.
[44] J. DeLucia, S.C. Jardin, A.M.M. Todd, An iterative metric method for solving the inverse tokamak equilibrium problem, Journal of Computational Physics, 37 (1980) 183-204.